Heterogeneous Catalysis

Deutsche Ausgabe: DOI: 10.1002/ange.201500454
Internationale Ausgabe: DOI: 10.1002/anie.201500454

High-Activity PtRuPd/C Catalyst for Direct Dimethyl Ether Fuel Cells**

*Qing Li, Xiaodong Wen, Gang Wu, Hoon T. Chung, Rui Gao, and Piotr Zelenay**

Abstract: *Dimethyl ether (DME) has been considered as a promising alternative fuel for direct-feed fuel cells but lack of an efficient DME oxidation electrocatalyst has remained the challenge for the commercialization of the direct DME fuel cell. The commonly studied binary PtRu catalyst shows much lower activity in DME than methanol oxidation. In this work, guided by density functional theory (DFT) calculation, a ternary carbon-supported PtRuPd catalyst was designed and synthesized for DME electrooxidation. DFT calculations indicated that Pd in the ternary PtRuPd catalyst is capable of significantly decreasing the activation energy of the C–O and C–H bond scission during the oxidation process. As evidenced by both electrochemical measurements in an aqueous electrolyte and polymer-electrolyte fuel cell testing, the ternary catalyst shows much higher activity (two-fold enhancement at 0.5 V in fuel cells) than the state-of-the-art binary $Pt_{50}Ru_{50}$/C catalyst (HiSPEC 12100).*

In recent years, much attention has been devoted to the direct methanol fuel cell (DMFC), a direct-feed fuel cell considered to be ideal for portable power applications due to the high energy density of the liquid fuel and ease of methanol storage and distribution compared to hydrogen. However, DMFC performance is limited by several factors, including the sluggish methanol oxidation kinetics and fuel crossover through the polymer electrolyte membrane.[1] Dimethyl ether (DME), a less toxic fuel than methanol, has been investigated in the last decade as a possible alternative fuel for the direct-feed fuel cells.[2] The theoretical open cell voltage (OCV) of the direct DME fuel cell (DDMEFC) is comparable to that of the DMFC (1.18 V vs. 1.21 V).[3] Upon oxidation to CO_2, a DME molecule releases 12 electrons, resulting in a higher energy density of DME than that of methanol (8.2 vs. 6.1 $kWh\,kg^{-1}$).[4] A lower DME dipole moment results in reduced fuel crossover compared to that of methanol, reducing the performance loss at the cathode caused by the formation of mixed potentials.[5]

In contrast to the direct-feed fuel cells operating on methanol, ethanol, and formic acid, the direct dimethyl ether fuel cell (DDMEFC) has not been studied to a great extent. The mechanism of DME oxidation has yet to be fully understood and catalysts designed specifically for the DDMEFC anode are yet to be developed. In situ infrared (IR) spectroscopy suggests that, similar to methanol, CO_{ads} is the dominant chemisorbed species of DME electrooxidation on Pt at low potentials.[6] Therefore, bimetallic Pt-based alloy catalysts capable of relieving the poisonous effect of CO_{ads}, such as PtRu, may be effective in DME oxidation.[7] To date, PtRu has been recognized as the state-of-the-art for the DDMEFC anode.[8] However, DME oxidation at PtRu remains kinetically impaired relative to that of methanol.[3] According to the mechanism proposed for DME oxidation on Pt,[5a,9] a high activation barrier for the C–O bond cleavage may be responsible for the slow kinetics of DME oxidation compared to that of methanol, as oxidation of chemisorbed species on Pt, such as CO_{ads}, is the same as that accepted for methanol oxidation. Since precious metals, such as Pd, are known to aid in the C–O bond cleavage of ethers,[10] the addition of Pd to the PtRu catalysts may enhance their catalytic activity in DME oxidation.

In this work, a carbon-supported $Pt_{46}Ru_{44}Pd_{10}$ catalyst for DME electrooxidation was rationally designed under the guidance of density functional theory (DFT) calculations. The Pt-to-Ru ratio was kept at 1:1 as $Pt_{50}Ru_{50}$ showed the better performance in the kinetic region of DDMEFC than other Pt-to-Ru ratios in our previous study.[3,11] The activity of the new ternary catalyst toward DME oxidation in an electrochemical cell and in a fuel cell was demonstrated to be superior to that of a commercial $Pt_{50}Ru_{50}$/C reference catalyst (HiSPEC 12100, Johnson Matthey). DFT was used to calculate the binding and activation energies of DME on $Pt_{47}Ru_{47}Pd_6$(111) and $Pt_{50}Ru_{50}$(111) systems (Supporting Information, SI). DFT calculations were also performed for four other catalysts: Pt(111), Pd(111), $Pt_{50}Pd_{50}$(111), and $Pt_{34}Ru_{33}Pd_{33}$(111) (Table S1). Of six calculated systems, the highest DME

[*] Dr. Q. Li, Prof. G. Wu,[++] Dr. H. T. Chung, Dr. P. Zelenay
Materials Physics and Applications Division
Los Alamos National Laboratory
Los Alamos, NM 87545 (USA)
E-mail: zelenay@lanl.gov
Prof. X. Wen[+]
Theoretical Division, Los Alamos National Laboratory
Los Alamos, NM 87545 (USA)
Dr. R. Gao
State Key Laboratory of Coal Conversion, Institute of Coal Chemistry, Chinese Academy of Sciences
P.O. Box 165, Taiyuan, Shanxi 030001 (PR China)
Prof. X. Wen,[+] Dr. R. Gao
Synfuels China
Beijing 100195 (PR China)
[+] Present address: State Key Laboratory of Coal Conversion
Institute of Coal Chemistry, Chinese Academy of Sciences
P.O. Box 165, Taiyuan, Shanxi 030001 (PR China)
[++] Present address: Department of Chemical and Biological Engineering
University at Buffalo, The State University of New York
Buffalo, NY 14260 (USA)

[**] Financial support from the DOE-EERE Fuel Cell Technologies Program (project ID: FC091) is gratefully acknowledged.
Supporting information for this article is available on the WWW under http://dx.doi.org/10.1002/anie.201500454.

binding energies and the lowest energy barriers for breaking both C–H and C–O bonds were obtained for two ternary catalysts, $Pt_{47}Ru_{47}Pd_6(111)$ and $Pt_{34}Ru_{33}Pd_{33}(111)$. Specifically, the calculated binding energies of DME on $Pt_{50}Ru_{50}(111)$ and $Pt_{47}Ru_{47}Pd_6(111)$ are −0.28 eV and −0.40 eV per one DME molecule, respectively (Figure S1). These results demonstrate that Pd doping enhances the binding energy of DME, which might be due to the electron-donating effect of Pd atoms. We scanned the potential energy for breaking C–O and C–H bonds in DME, as shown in Figure 1. The calculated

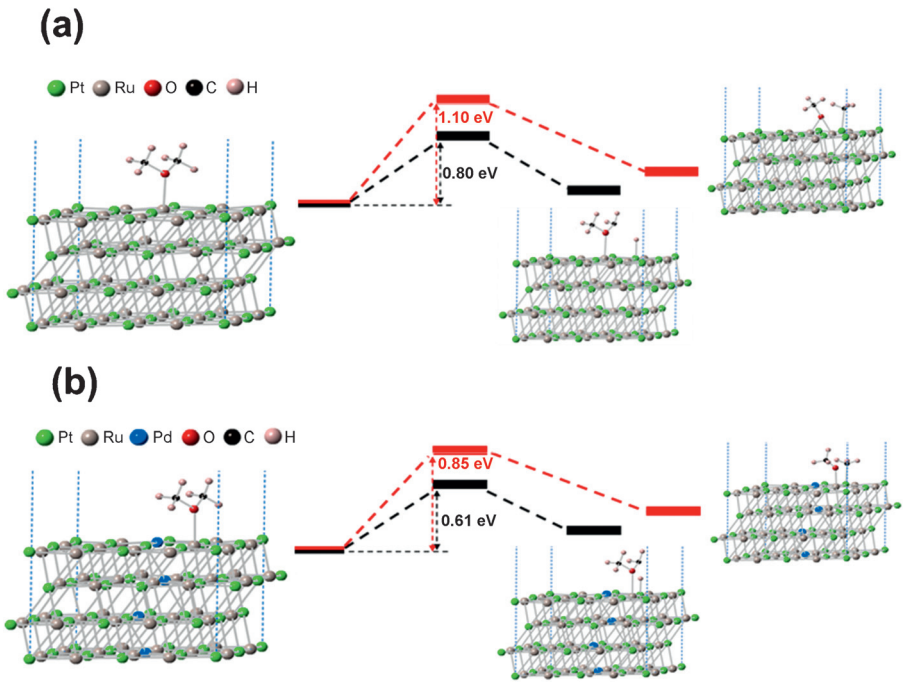

Figure 1. Activation energies for breaking C–O (red) and C–H (black) bonds in DME oxidation on $Pt_{50}Ru_{50}(111)$ and $Pt_{47}Ru_{47}Pd_6(111)$.

activation energies for breaking C–O bond on $Pt_{50}Ru_{50}(111)$ and $Pt_{47}Ru_{47}Pd_6(111)$ are 1.1 eV and 0.85 eV, respectively. This indicates that Pd doping decreases the energy of the C–O bond. In addition, Pd addition to PtRu also significantly lowers the activation energy for C–H bond scission during DME oxidation by 0.19 eV (Figure 1). However, a comparison of the bond breaking energy at $Pt_{47}Ru_{47}Pd_6(111)$ and $Pt_{34}Ru_{33}Pd_{33}(111)$, 0.85 eV versus 1.17 eV for the C–O bond and 0.61 eV versus 0.78 eV for the C–H bond (Figure S2), indicates that "overdoping" of PtRu catalysts with Pd may outweigh the ternary catalyst benefits in DME oxidation.

The $Pt_{46}Ru_{44}Pd_{10}$/C catalyst was synthesized by a modified polyol method.[12] During the synthesis, $H_2PtCl_6{\cdot}6H_2O$, $RuCl_3$, and $PdCl_2$ in desired ratios were employed as metal precursors and ethylene glycol was used as a solvent and reducing agent at the same time. The mixture was then heated up and maintained at 170 °C for 3 h to enable complete reduction of metals. After that, carbon black (XC-72) was introduced to yield carbon-supported PtRuPd nanoparticles (NPs; see SI for details). The characteristics of the as-synthesized PtRuPd/C catalyst and $Pt_{50}Ru_{50}$/C are summarized in Table S2. The total metal loading in the PtRuPd/C catalyst is as high as 67 %, as determined by thermogravimetric analysis (TGA). The metal loading values for PtRu/C catalysts were typically lower than 40 wt % due to the challenge in achieving uniform NP dispersion at higher metal loadings. Because of generally sluggish kinetics of the oxidation process and the need not to obstruct fuel transport in the electrode, the direct-feed fuel cell anode use high catalyst loadings and relatively high metal-to-carbon ratios to achieve an acceptable performance.[13] In this work, the metal content in the PtRuPd/C catalysts is similar to that in the binary $Pt_{50}Ru_{50}$/C catalyst (73 wt %). The Pt:Ru:Pd atomic ratio was determined to be 46:44:10 by X-ray fluorescence (XRF). The PtRuPd alloy particle size, calculated from the Pt(111) XRD peak using the Debye–Scherrer equation,[14] is around 3.2 nm. It is slightly smaller than in the $Pt_{50}Ru_{50}$/C catalysts (3.6 nm). The surface area, estimated from crystallite size for PtRuPd/C ($60\ m^2/g_{metal}$), exceeds that of $Pt_{50}Ru_{50}$/C ($49\ m^2/g_{metal}$).

XRD patterns for Pt/C (HiSPEC 9100), $Pt_{50}Ru_{50}$/C (HiSPEC 12100), and $Pt_{46}Ru_{44}Pd_{10}$/C catalysts are shown in Figure 2a. All three catalysts exhibit a face-centered cubic (fcc) crystal structure, with diffraction peaks at approximately 39.5°, 46.1°, and 67.7° for (111), (200), and (220) planes, respectively. The formation of an alloy structure in the $Pt_{46}Ru_{44}Pd_{10}$/C catalyst is confirmed by the (111) peak shift relative to

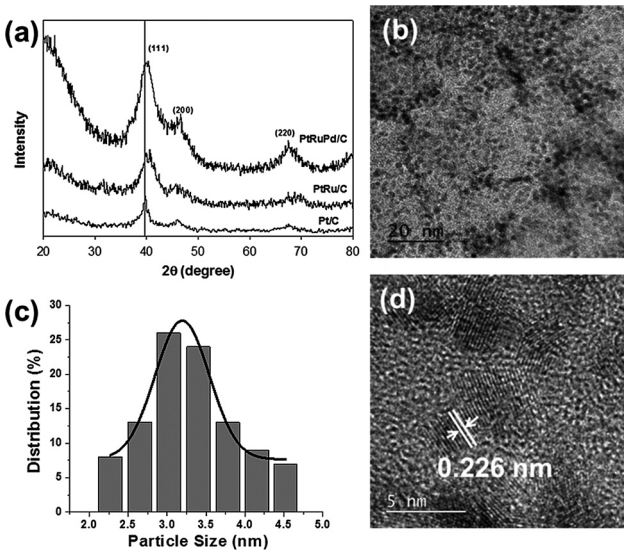

Figure 2. a) XRD patterns of the $Pt_{46}Ru_{44}Pd_{10}$/C, $Pt_{50}Ru_{50}$/C (HiSPEC 12100) and Pt/C (HiSPEC 9100) catalysts. b) TEM image, c) particle size distribution, and d) HR-TEM image of $Pt_{46}Ru_{44}Pd_{10}$/C.

pure Pt. Furthermore, the (111) peak for $Pt_{46}Ru_{44}Pd_{10}/C$ is shifted slightly to lower 2θ values compared to those for $Pt_{50}Ru_{50}/C$, likely due to a larger atomic radius of Pd than Ru (atomic radii: $r_{Pt} = 1.39$ Å, $r_{Ru} = 1.34$ Å, $r_{Pd} = 1.37$ Å). The SEM images of $Pt_{46}Ru_{44}Pd_{10}/C$ and $Pt_{50}Ru_{50}/C$ are presented in Figure S3, indicating similar morphology of the two catalysts. TEM images (Figures 2b and S4) also show that PtRuPd NPs are uniformly dispersed on carbon supports without agglomeration, even at a high metal loading of 67 wt%. The particle size distribution is relatively narrow (Figure 2c), with an average particle size of ca. 3.3 nm, which is in good agreement with the crystallite size calculated from XRD patterns. $Pt_{40}Ru_{40}Pd_{20}/C$ and $Pt_{34}Ru_{33}Pd_{33}/C$ catalysts also exhibit uniform particle dispersion on carbon and a narrow particle size distribution (Figure S5). The average particle sizes in $Pt_{40}Ru_{40}Pd_{20}/C$ and $Pt_{34}Ru_{33}Pd_{33}/C$ are ca. 3.2 nm and 3.4 nm, respectively. In contrast, particle agglomeration is observed in commercial $Pt_{50}Ru_{50}/C$ catalyst (Figure S4). The HR-TEM image in Figure 2d demonstrates that $Pt_{46}Ru_{44}Pd_{10}$ NPs are highly crystalline. The measured lattice spacing of about 0.226 nm corresponds to the (111) plane of PtRuPd alloy. This value is between the lattice spacing for the (111) planes in Pt (0.228 nm) and PtRu alloy (0.223 nm),[15] corroborating Pd incorporation into PtRu crystal lattice.

Steady-state polarization plots and cyclic voltammograms measured in DME-saturated 0.1 M $HClO_4$ ($C_{DME} = \approx 0.74$ M, corrected for the altitude of Los Alamos[16]) are shown in Figures 3a and S6, respectively. They attest to higher activity of the ternary $Pt_{46}Ru_{44}Pd_{10}/C$ catalyst than the binary $Pt_{50}Ru_{50}/C$ reference catalyst. The onset potential of DME oxidation on $Pt_{46}Ru_{44}Pd_{10}/C$ in steady-state polarization plots is by ca. 70 mV lower than on $Pt_{50}Ru_{50}/C$ (0.36 V vs. 0.43 V). The observed broad oxidation peak on the $Pt_{46}Ru_{44}Pd_{10}/C$ catalyst is attributed to the oxidation of CO_{ad} and $(\text{-CHO})_{ad}$.[3] In contrast, no significant DME oxidation peak is observed on $Pt_{50}Ru_{50}/C$ at room temperature. The oxidation current decreases at potentials more positive than 0.9 V, i.e., in the region where the Pt surface undergoes more significant oxidation, it becomes less active for DME oxidation. The electrochemical data attest to the enhancement in the kinetics of DME oxidation once Pd is added to PtRu catalysts. This effect is most likely due to the activating effect of Pd on the C–O and C–H bond breaking.

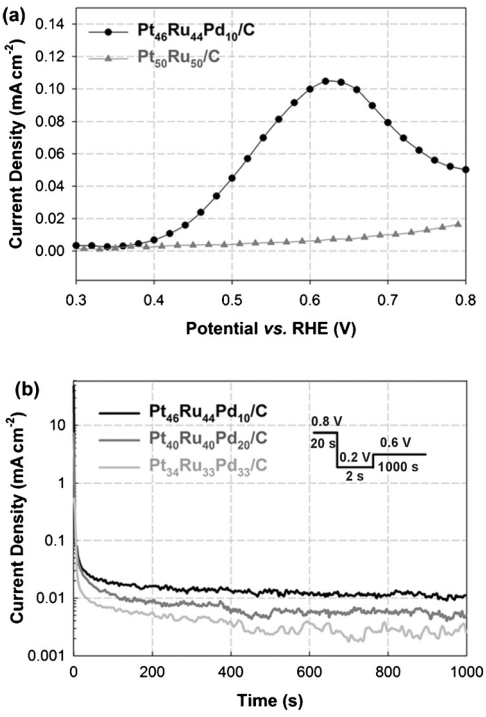

Figure 3. a) Steady-state polarization plots of DME oxidation on $Pt_{46}Ru_{44}Pd_{10}/C$ and $Pt_{50}Ru_{50}/C$ in 0.74 M DME + 0.1 M $HClO_4$ at a room temperature. b) DME oxidation under constant-potential conditions on three different PtRuPd/C catalysts at 0.6 V.

To gain further insight into the DME oxidation mechanism, experiments were performed that involved oxidative removal of the surface species derived from DME (DME stripping in SI). As shown in Figure S7, hydrogen adsorption in the potential region from 0.05 to 0.4 V is suppressed following DME adsorption (chemisorption) on the catalyst surface. Similar onset potential values of CO (dominant species from IR spectroscopy studies[6]) oxidation on both catalysts indicate that Pd addition to the binary PtRu catalyst does not improve the kinetics of CO oxidation. The Q_{ox} value (the oxidation charge of chemisorbed CO) is much larger for $Pt_{46}Ru_{44}Pd_{10}/C$ than for $Pt_{50}Ru_{50}/C$ (1.53 mC cm^{-2} vs. 0.92 mC cm^{-2}), indicating higher coverage by adsorbed CO on $Pt_{46}Ru_{44}Pd_{10}/C$ and more efficient C–O bond cleavage in the presence of Pd. The addition of Pd may affect the effectiveness of CO oxidation by Ru due to lowering Ru content in the catalyst. Even if some inhibition of the CO removal is taking place, the results show that the activation of C–O and C–H bond scission by Pd significantly benefits the overall rate of DME oxidation.

The dependence of metal composition in PtRuPd/C catalysts on the activity was also studied by chronoamperometry. Figure 3b shows the activity of DME oxidation as a function of time at a constant potential of 0.6 V on PtRuPd/C catalysts as a function of catalyst composition. After holding the potential at 0.8 V for 20 s to clean the surface, the potential was changed back to 0.2 V for 2 s and then stepped up to 0.6 V for 1000 s. The maximum current value on all catalysts was reached immediately after the latter step, followed by a gradual decrease in current for about 2 min, until a steady state was reached. The measured steady-state currents for the three catalysts decreased in the following order: $Pt_{46}Ru_{44}Pd_{10}/C > Pt_{40}Ru_{40}Pd_{20}/C > Pt_{34}Ru_{33}Pd_{33}/C$. The addition of 10 at% Pd turned out to assure efficient C–O bond scission without significantly inhibiting the removal of CO_{ad} by Ru hydroxide/oxides. In the case of a higher Pd content, the beneficial role of Pd was offset by the "dilution" of the Pt and Ru sites on the catalyst surface and ensuing drop in the overall performance of the ternary catalyst.

DDMEFC polarization plots recorded with $Pt_{46}Ru_{44}Pd_{10}/C$ and $Pt_{50}Ru_{50}/C$ at the same Pt loading (2.7 mg_{Pt}/cm^2) in the anode are shown in Figure 4a. The OCV measured with $Pt_{46}Ru_{44}Pd_{10}/C$ is by 25 mV higher than that measured with $Pt_{50}Ru_{50}/C$ (0.875 V vs. 0.850 V). The cell voltage measured with $Pt_{46}Ru_{44}Pd_{10}/C$ at 0.15 A cm^{-2} is by ca. 70 mV higher than that measured with $Pt_{50}Ru_{50}/C$. Noteworthy, the new catalyst

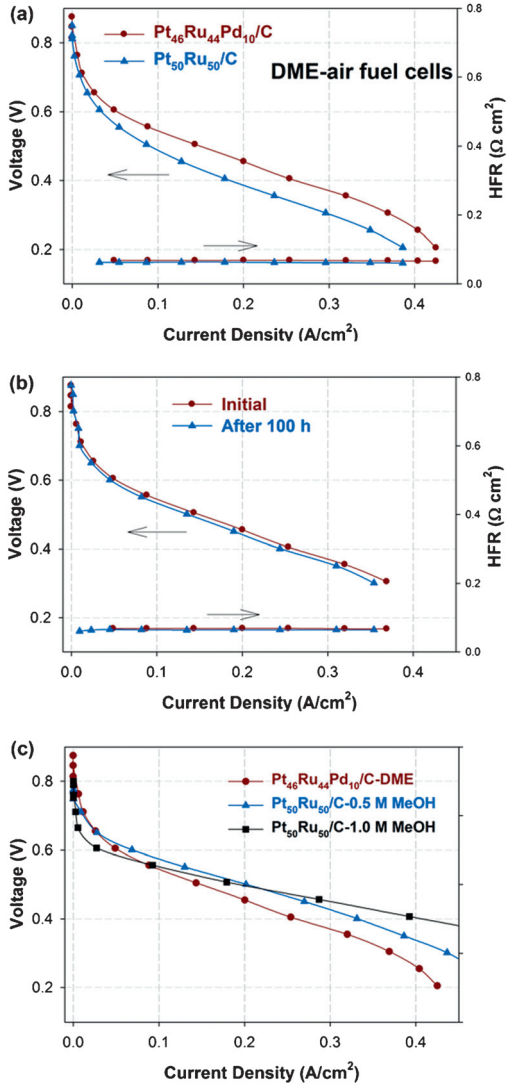

Figure 4. a) DDMEFC polarization plots recorded with $Pt_{46}Ru_{44}Pd_{10}/C$ and $Pt_{50}Ru_{50}/C$ catalysts. b) The durability test of DDMEFC recorded with $Pt_{46}Ru_{44}Pd_{10}/C$ catalyst. c) Performance comparison of DDMEFC and DMFC operated under their respective optimum conditions. DDMEFC operating conditions: anode—2.7 $mg_{Pt}\,cm^{-2}$ ($Pt_{46}Ru_{44}Pd_{10}/C$ or HiSPEC 12100), 40 sccm DME gas, 0.21 MPa; cathode—2.0 $mg\,cm^{-2}$ Pt/C, 500 sccm air, 0.14 MPa; membrane—Nafion 212; cell temperature—80 °C. The operating conditions for DMFC: anode—2.7 $mg_{Pt}\,cm^{-2}$ HiSPEC 12100, 1.8 $mL\,min^{-1}$ 0.5 M or 1.0 M MeOH, 0 MPa; cathode—2.0 $mg_{Pt}\,cm^{-2}$ Pt/C, 100 sccm air, 0.14 MPa; membrane—Nafion 115; cell temperature—80 °C.

does not suffer from a mass transport penalty due to the relatively high metal loading. Anode polarization plots in Figure S8 also confirm higher activity of $Pt_{46}Ru_{44}Pd_{10}/C$ than that of $Pt_{50}Ru_{50}/C$. DDMEFC test data show that ternary PtRuPd/C catalysts offer significant performance advantage over the binary PtRu/C formulations due to the activating effect of Pd on the C–O and C–H bond cleavage. The DDMEFC current density achieved in this study at a "standard" voltage of 0.5 V is approximately 100% higher than the best performance published to date.[17] The DDMEFC performance reported in publications dating back to 2005 are summarized in Table S3.

Performance durability of the $Pt_{46}Ru_{44}Pd_{10}/C$ catalyst was evaluated in a DDMEFC at a constant operating voltage of 0.4 V (Figure 4b). After 100 h of operation no significant performance loss was observed. Finally, the performance of a DDMEFC with $Pt_{46}Ru_{44}Pd_{10}/C$ anode was compared to that of a state-of-the-art DMFC (Figure 4c). With both systems operating under their respective optimum conditions, the DDMEFC performance was found superior to that of the DMFC at cell voltages above 0.65 V when the reference DMFC system was operated at a methanol concentration of 0.5 M and above 0.55 V when methanol feed concentration was 1.0 M. (These two methanol concentrations are commonly used with DMFCs, depending on whether the fuel conversion efficiency or maximum power are the primary requirement.) This result establishes the DDMEFC as a serious competitor of the DMFC for portable and mobile power applications.

To summarize, a new type of $Pt_{46}Ru_{44}Pd_{10}/C$ catalyst was developed by a modified polyol method to improve the kinetics of DME electrooxidation relative to the commercial $Pt_{50}Ru_{50}/C$ catalyst. A high metal loading of up to 67 wt% was targeted to maximize catalysts performance without a mass transport penalty. An addition of 10 at% Pd to the PtRu catalyst was found to enhance the rate of the C–O bond scission without noticeably inhibiting the removal of surface CO by Ru hydroxide/oxides. Compared to the state-of-the-art $Pt_{50}Ru_{50}/C$ HiSPEC 12100 catalyst (Johnson Matthey), the $Pt_{46}Ru_{44}Pd_{10}/C$ catalyst exhibits lower onset potential for DME oxidation in electrochemical measurements and higher OCV and better performance in the kinetic region in DDMEFC testing. The achieved DME fuel cell performance at a viable fuel cell voltage of 0.5 V is by a factor of approximately two higher than the best performance reported before and slightly surpassing that of a state-of-the-art DMFC. DFT calculations indicate that Pd addition to the PtRu alloy increases the binding energy of DME on catalyst surface and decreases the breaking energy for C–O and C–H bonds. Further optimization of the composition, morphology and structure of ternary PtRuPd catalysts will be the focus of an upcoming report.

Keywords: dimethyl ether · electrochemical oxidation · fuel cells · heterogeneous catalysis · nanoparticles

How to cite: *Angew. Chem. Int. Ed.* **2015**, *54*, 7524–7528
Angew. Chem. **2015**, *127*, 7634–7638

[1] M. Ahmed, I. Dincer, *Int. J. Energy Res.* **2011**, *35*, 1213–1228.
[2] J. O. Jensen, A. Vassiliev, M. I. Olsen, Q. F. Li, C. Pan, L. N. Cleemann, T. Steenberg, H. A. Hjuler, N. J. Bjerrum, *J. Power Sources* **2012**, *211*, 173–176.
[3] Q. Li, G. Wu, C. M. Johnston, P. Zelenay, *Electrocatalysis* **2014**, *5*, 310–317.
[4] Q. Li, G. Wu, Z. X. Bi, C. M. Johnston, P. Zelenay, *ECS Trans.* **2013**, *50*, 1933–1941.
[5] a) J. T. Müller, P. M. Urban, W. F. Holderich, K. M. Colbow, J. Zhang, D. P. Wilkinson, *J. Electrochem. Soc.* **2000**, *147*, 4058–4060; b) I. Mizutani, Y. Liu, S. Mitsushima, K. I. Ota, N. Kamiya, *J. Power Sources* **2006**, *156*, 183–189.
[6] Y. Liu, M. Muraoka, S. Mitsushima, K. I. Ota, N. Kamiya, *Electrochim. Acta* **2007**, *52*, 5781–5788.

[7] Y. Liu, S. Mitsushima, K. Ota, N. Kamiya, *Electrochim. Acta* **2006**, *51*, 6503 – 6509.
[8] A. Serov, C. Kwak, *Appl. Catal. B* **2009**, *91*, 1 – 10.
[9] E. Y. Votchenko, M. S. Kubanova, N. V. Smirnova, O. A. Petrii, *Russ. J. Electrochem.* **2010**, *46*, 212 – 217.
[10] R. A. Widenhoefer, H. A. Zhong, S. L. Buchwald, *J. Am. Chem. Soc.* **1997**, *119*, 6787 – 6795.
[11] Q. Li, G. Wu, C. M. Johnston, P. Zelenay, *ECS Trans.* **2011**, *41*, 1969 – 1977.
[12] G. Wu, R. Swaidan, D. Li, N. Li, *Electrochim. Acta* **2008**, *53*, 7622 – 7629.
[13] a) G. Wu, D. Li, C. Dai, D. Wang, N. Li, *Langmuir* **2008**, *24*, 3566 – 3575; b) S. Y. Yan, G. Q. Sun, J. Tian, L. H. Jiang, J. Qi, Q. Xin, *Electrochim. Acta* **2006**, *52*, 1692 – 1696.
[14] a) V. Radmilovic, H. A. Gasteiger, P. N. Ross, *J. Catal.* **1995**, *154*, 98 – 106; b) M. Umeda, H. Ojima, M. Mohamedi, I. Uchida, *J. Power Sources* **2004**, *136*, 10 – 15.
[15] J. S. Guo, G. Q. Sun, Z. M. Wu, S. G. Sun, S. Y. Yan, L. Cao, Y. S. Yan, D. S. Su, Q. Xin, *J. Power Sources* **2007**, *172*, 666 – 675.
[16] M. H. Shao, J. Warren, N. S. Marinkovic, P. W. Faguy, R. R. Adzic, *Electrochem. Commun.* **2005**, *7*, 459 – 465.
[17] J. Y. Im, B. S. Kim, H. G. Choi, S. M. Cho, *J. Power Sources* **2008**, *179*, 301 – 304.

Received: January 16, 2015
Revised: March 30, 2015
Published online: May 12, 2015

